Transcranial ultrasonic propagation and enhanced brain imaging exploiting the focusing effect of the skull

Stamatis A. Amanatiadis
Department of Electrical and Computer Engineering, Aristotle University of Thessaloniki, Thessaloniki, Greece and Ormylia Foundation, Art Diagnosis Center, Ormylia, Greece

Georgios K. Apostolidis
Department of Electrical and Computer Engineering, Aristotle University of Thessaloniki, Thessaloniki, Greece

Chrysanthi S. Bekiari
Faculty of Veterinary Medicine, Aristotle University of Thessaloniki, Thessaloniki, Greece, and

Nikolaos V. Kantartzis
Department of Electrical and Computer Engineering, Aristotle University of Thessaloniki, Thessaloniki, Greece

Received 6 October 2019
Revised 2 March 2020
Accepted 2 May 2020

Abstract

Purpose – The reliable transcranial imaging of brain inner structures for diagnostic purposes is deemed crucial owing to the decisive importance and contribution of the brain in human life. The purpose of this paper is to investigate the potential application of medical ultrasounds to transcranial imaging using advanced techniques, such as the total focussing method.

Design/methodology/approach – Initially, the fundamental details of the total focussing method are presented, while the skull properties, such as the increased acoustic velocity and scattering, are thoroughly examined. Although, these skull characteristics constitute the main drawback of typical transcranial ultrasonic propagation algorithms, they are exploited to focus the acoustic waves towards

Acknowledgment

Operational Programme
Human Resources Development, Education and Lifelong Learning
Co-financed by Greece and the European Union

This research is co-financed by Greece and the European Union (European Social Fund – ESF) through the Operational Program "Human Resources Development, Education and Lifelong Learning 2014-2020" in the context of the project "Design of a non-invasive system for brain defect detection using ultrasonography" (MIS 5005360).

COMPEL - The international journal for computation and mathematics in electrical and electronic engineering

0332-1649
DOI 10.1108/COMPEL-10-2019-0387

the brain. To this goal, a virtual source is designed, considering the wave refraction, to efficiently correct the reconstructed brain image. Finally, the verification of the novel method is conducted through numerical simulations of various realistic setups.

Findings – The theoretically designed virtual source resembles a focussed sensor; therefore, the directivity increment, owing to the propagation through the skull, is confirmed. Moreover, numerical simulations of real-world scenarios indicate that the typical artifacts of the conventional total focussing method are fully overcome because of the increased directivity of the proposed technique, while the reconstructed image is efficiently corrected when the proposed virtual source is used.

Originality/value – A new systematic methodology along with the design of a flexible virtual source is developed in this paper for the reliable and precise transcranial ultrasonic image reconstruction of the brain. Despite the slight degradation owing to the skull scattering, the combined application of the total focussing method and the featured virtual source can successfully detect arbitrary anomalies in the brain that cannot be spotted by conventional techniques.

Keywords Brain imaging, Synthetic aperture, Total focussing method, Transcranial imaging, Ultrasonics, Virtual source

Paper type Research paper

1. Introduction

Brain imaging is one of the most crucial and rapidly evolving sectors in medical applications owing to the vital contribution of the brain in human life. The reliable imaging of the brain for diagnostic purposes is a very significant procedure, as the early detection of possible anomalies is deemed decisive for a successful therapy. Several defects and malfunctions in the brain's inner structure can be spotted through various non-invasive imaging techniques (Oldendorf, 1978; Wintermark *et al.*, 2005; Shenton *et al.*, 2012; Kraiger and Schnizer, 2013; Zhang *et al.*, 2014; Szajerman *et al.*, 2018; Eichardt *et al.*, 2019) either considering the different properties of the brain tissues or through the brain activity. The former includes the popular magnetic resonance imaging (MRI) and the computed tomography (CT) scanning, while the latter is implemented in terms of functional MRI (fMRI), positron emission tomography (PET), electroencephalography (EEG) and magnetoencephalography (MEG). Although, each method has specific advantages, such as the high resolution of MRI, CT, fMRI and PET or the very fast temporal response of EEG and MEG, there are some considerable disadvantages, such as the expensive implementation and the low resolution of the resulting image.

Apart from the prior approaches, the diagnostic ultrasound method has become one of the most popular non-invasive imaging techniques. Ultrasonic imaging is based on the propagation of acoustic waves and the tomographic reconstruction because of the multiple reflections of the inner details. It is a very safe, economic and accurate non-destructive process with applications in several medical examinations that include abdominal, heart and other soft body parts. Despite its merits, ultrasonography has a limited use in human brain imaging, compared to other methods, owing to the physically hard-structured skull that deteriorates brain-imaging resolution. In particular, the acoustic properties of a material depend on its elasticity and density, and consequently, the bones exhibit considerably different attributes compared to other soft tissues. Thus, the propagation of an acoustic wave beyond a bone, such as the brain, is severely degraded because of the skull's scattering properties. Nevertheless, there are some approaches that involve ultrasonic waves either for therapeutic or imaging purposes. An interesting case, regarding the therapeutic ultrasound, is its focussing on specific brain areas, facilitated via the inherent skull feature to concentrate acoustic

waves (Clement and Hynynen, 2002; Hölscher *et al.*, 2008). However, ultrasonic image reconstruction is a more complex procedure, and thus the exact positioning of acoustic wave focussing is MR-guided – an overall expensive process as above-mentioned.

On the other hand, concerning the imaging, that is the topic of this work, there are studies that conventional ultrasound techniques are able to detect regions of interest through simple image processing algorithms (Behnke *et al.*, 2005; Hölscher *et al.*, 2005) or the application of transducers to opposite skull sides (Vignon *et al.*, 2005; Vignon *et al.*, 2006; Lindsey *et al.*, 2011). It is noteworthy to indicate that the ultrasonic probe in such techniques is placed at the posterior or middle temporal bone window, where the thickness of the skull is minimum (Berg and Becker, 2002; Godau and Berg, 2010). This fact limits the imaging procedure, and only certain brain regions can be visualised, specifically the mesencephalic ones, while the resolution is somewhat degraded.

In this paper, the acoustic properties of the skull are exploited and incorporated in the powerful total focussing method (TFM) (Holmes *et al.*, 2004; Zhang *et al.*, 2010; Le Jeune *et al.*, 2015) along with the equivalent synthetic aperture imaging technique (Lockwood *et al.*, 1998; Bae and Jeong, 2000; Jensen *et al.*, 2006) to acquire precise tomographic brain images. Explicitly, the skull tends to focus a spherically propagating acoustic wave, and the individual element directivity is increased, avoiding the inherent artifacts of the conventional TFM. In this paper, this significant feature is exploited to enhance transcranial brain imaging through the effective design of virtual sources, considering the increased acoustic velocity of the skull. Finally, the novel approach is validated on two diverse realistic setups that are numerically analysed by means of the efficient *k*-space algorithm (Tabei *et al.*, 2002; Mast *et al.*, 2001).

2. Formulation of the total focussing method

2.1 Operation principle

The key principle of the TFM is the acquisition of various low-resolution images and their appropriate fusion to a high quality one. Particularly, in TFM, an array of N transducers is used, and at each time step, only one array element is transmitting a nearly spherical ultrasonic wave. The latter is propagating towards the area of investigation, and the back-scattered signals, owing to reflections at discontinuities of the structure, are received by every array element. This procedure continues until all transducers are stimulated, and the full matrix capture (FMC) is assembled as follows:

$$\begin{bmatrix} a_{1,1} & a_{1,2} & a_{1,3} & \cdots & a_{1,N} \\ a_{2,1} & a_{2,2} & a_{2,3} & \cdots & a_{2,N} \\ a_{3,1} & a_{3,2} & a_{3,3} & \cdots & a_{3,N} \\ \vdots & \vdots & \vdots & \ddots & \vdots \\ a_{N,1} & a_{N,2} & a_{N,3} & \cdots & a_{N,N} \end{bmatrix}, \tag{1}$$

with $a_{i,j}$ the A-scan for the transmitting element j to the receiving one i, where $i,j = 1, 2, \ldots, N$. An indicative example of an FMC is depicted in Figure 1, where the various A-scans are located at the corresponding positions of equation (1).

Then, the acquired data, stored in the FMC, are properly processed to obtain the images of the region under study. The latter is discretised, as illustrated in Figure 2, and an image I_j

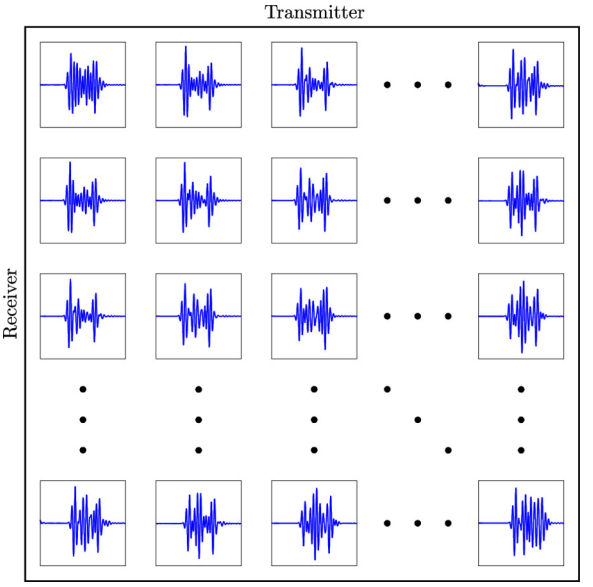

Figure 1.
A-scans inside a FMC

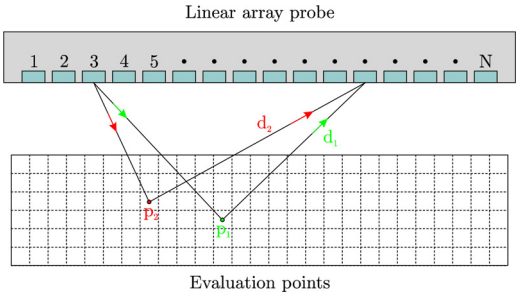

Figure 2.
Main operation principle of the TFM; distances d_1 and d_2 are identical, hence resulting in possible artifacts

is formed for the transmitted wave j via the summation of the intensities in the equivalent column of equation (1), i.e.

$$I_j(x,y) = \sum_{i=1}^{N} a_{i,j}\left[t_{i,j}(x,y)\right], \tag{2}$$

where $t_{i,j}$ (x,y) is the time-of-flight (TOF) from the transmitted element j to the desired evaluation point (x, y) and finally to the receiver i:

$$t_{i,j}(x,y) = \frac{d_{i,j}(x,y)}{c_{\text{ref}}}, \tag{3}$$

where c_{ref} is the reference acoustic velocity,

$$d_{i,j}(x,y) = \sqrt{(x_i - x)^2 + (y_i - y)^2} + \sqrt{(x_j - x)^2 + (y_j - y)^2}, \tag{4}$$

and (x_i, y_i) and (x_j, y_j) are the position of the receiver and transmitter, respectively. Note that the deviation from c_{ref} for the majority of the scenarios, not including the skull though, is negligible (less than 10%), and its constant value approximation provides adequate results.

The aforementioned scheme is realised for every transmitting element to create N images, whereas the primary point in this procedure is that the application of different time delays to each signal, namely, the evaluation of the TOF $t_{i,j}$ (x,y), practically leads to dynamic focussing. However, each individual image is considered to be of low quality, owing to the insonification of the involved spherical waves. For this reason, image fusion techniques are selected to synthesise the final high-resolution image I_{HQ} with the desired dynamic focussing. Although, there are several algorithms, the most convenient one, implemented herein, performs the direct summation of all individual images:

$$\text{I}_{\text{HQ}}(x, y) = \sum_{j=1}^{N} I_j(x,y). \tag{5}$$

Despite the fact that the TFM features are identical for high precision ultrasonic imaging, the spherically propagating transmitted wave generates some noticeable artifacts. In particular, the TOF of a transmitter – receiver pair can be identical for different evaluation points, as depicted in Figure 2 for points $p_1(x_1, y_1)$ and $p_2(x_2, y_2)$, where $d_1 \equiv d_2$. Moreover, the acoustic wave propagates spherically, and thus a unidirectional pattern is acquired, resulting in:

$$a_{i,j}\left[t_{i,j}(x_1,y_1)\right] \equiv a_{i,j}\left[t_{i,j}(x_2,y_2)\right]. \tag{6}$$

As a consequence, any possible reflection, because of the inner structure, is recorded at various non-physical positions hence generating various artifacts. Observe that the summation of the different signals in equation (2) is an attempt to degrade these artifacts, as adjacent elements tend to mutually annihilate them. Nonetheless, they are not completely eliminated, which can typically lead to a completely misleading diagnosis.

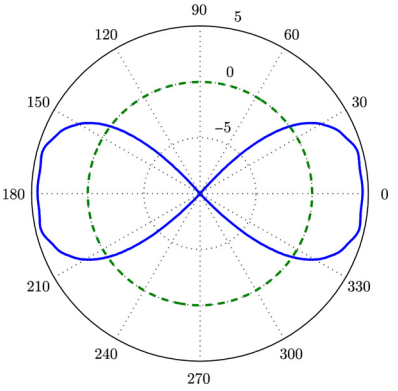

Figure 3.
Directivity of a single source spherical wave (a) at the free space (dashed line) and (b) when skull is inserted at both sides (continuous line)

2.2 Transcranial imaging exploiting skull focussing

As already mentioned, transcranial ultrasonic imaging is, in general, avoided owing to the skull structure. The latter is significantly more reflective because of its increased acoustic velocity, than the coupling materials and the brain tissues, as well as rather absorbent owing to its scattering nature. Inevitably, these characteristics prevent the efficient propagation of acoustic waves in the brain; therefore, conventional ultrasonic imaging is poor. Nevertheless, the use of advanced techniques, such as the TFM, can enhance the acquired images by means of dynamic focussing. Additionally, the acoustic properties of the skull introduce some interesting effects, particularly the intrinsic focus of a transmitted wave that may be exploited to further improve the imaging. Indeed, the directivity of a single-source spherical wave is constant at any direction in contrast to the directive propagation in the presence of the skull. This phenomenon is demonstrated in Figure 3, where at the latter case, the maximum observed directivity is almost 5dBi.

Despite the desired directivity, attributed to the skull, its acoustic velocity deviates considerably from the reference one. Specifically, c_{ref} is selected equal to the sound of speed in water, i.e. 1,500 m/s, as most of the coupling materials and brain tissues exhibit equivalent values. This is not the case for the skull, though, whose acoustic velocity c_{skull} deviates from c_{ref} by almost 80%. Consequently, a correction of the conventional scheme is required via the formation of a virtual source, where the position of the elements is estimated by considering the increased c_{skull}, as presented in Figure 4. The term "virtual" is introduced, as no additional sources are inserted, yet the original ones are virtually displaced. The angle of approach θ_i from the array element i at point (x_i, y_i) to the evaluation point (x, y) is used to calculate the propagation angle θ_t in the skull via Snell's law as following:

$$\theta_t = \frac{\pi}{2} - \sin^{-1}\left(\frac{c_{\text{skull}}}{c_{\text{ref}}}\sin\theta_i\right), \tag{7}$$

Next, the total distance d_{skull} inside the skull is estimated in terms of its thickness, w, yielding:

$$d_{\text{skull}} = w/\sin\theta_t. \tag{8}$$

Notice that the thickness can be easily measured, prior to the imaging process, through the ISO 16809 standard (International Organization for Standardization ISO, 2019). Finally, the total distance d_{total} is computed in the form of the following:

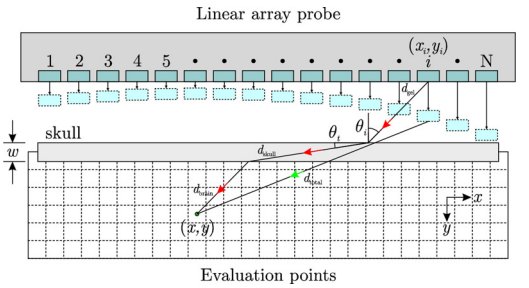

Figure 4.
Virtual source owing to the high acoustic velocity of the human skull

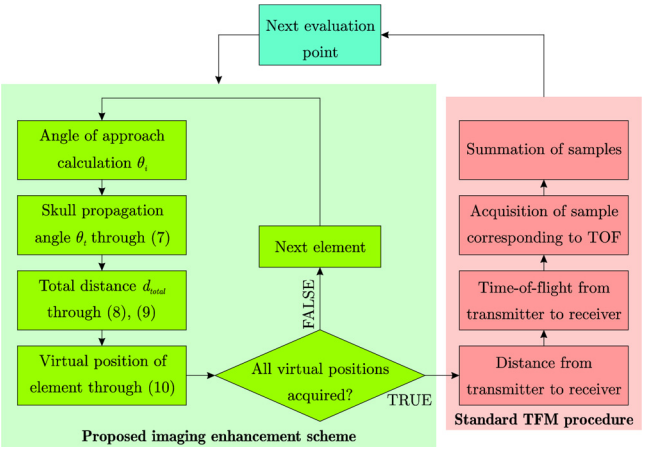

Figure 5. Algorithmic procedure of the proposed methodology

$$d_{\text{total}} = d_{\text{gel}} + \frac{c_{\text{ref}}}{c_{\text{skull}}} d_{\text{skull}} + d_{\text{brain}}, \tag{9}$$

where d_{gel} and d_{brain} are the distance that acoustic waves propagate in the coupling material and the brain, respectively. The virtual position of element i is, now, located at (x'_i, y'_i), namely,

$$x'_i \equiv x_i \quad \text{and} \quad y'_i \equiv y - \sqrt{d_{\text{total}}^2 - x_i^2}\,. \tag{10}$$

One interesting observation is that the virtual positions are closer to the skull, so forming an array that resembles a focussed source. The complete algorithmic procedure of the proposed methodology for the transcranial ultrasound enhanced imaging method is depicted in the flowchart of Figure 5.

3. Numerical validation

The verification of the new method, which combines the incorporation of the TFM with the development of a virtual source, is investigated via numerical analysis of realistic setups. All simulations are conducted through the precise *k*-Wave MATLAB® toolbox because of the flexibility and efficiency of the *k*-space algorithm (Treeby and Cox, 2010). Furthermore, the computational domain is discretised in $256 \times 256 \times 256$ cubic cells with a spatial increment of $\Delta x = \Delta y = \Delta z = 156\,\mu$m, while the time-step is set to 31 ns, and the open

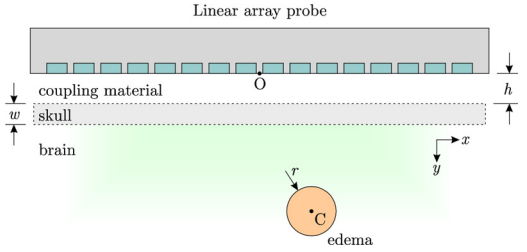

Figure 6. Simulation setup of the first scenario that includes an edema scatterer

boundaries are truncated by means of a 16-cell thick perfectly matched layer absorbing boundary condition.

3.1 Spherical edema scatterer

The first configuration is displayed in Figure 6 and comprises a 64-element linear array and a spherical edema scatterer of radius r = 3mm, centred at point C (6.25 mm, 22.75 mm) relatively to the origin O (0,0), with an acoustic velocity of 1,700 m/s. Moreover, the popular hydrogel is chosen as our coupling material with c_{ref} = 1,540 m/s, while a 5 mm thick skull of

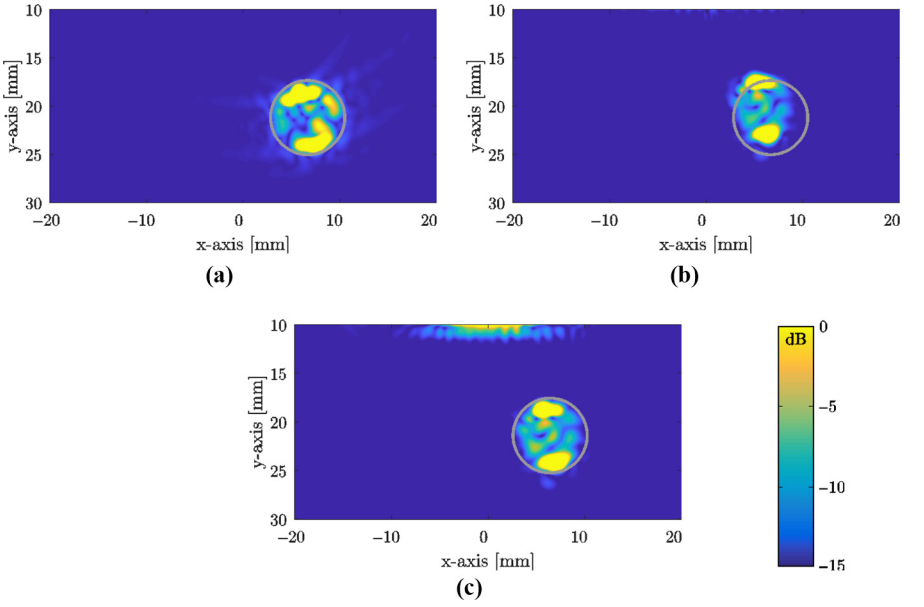

Figure 7.
Image reconstruction of the setup in Figure 6 using (a) the conventional TFM scheme without the skull, (b) with the skull and (c) the proposed scheme

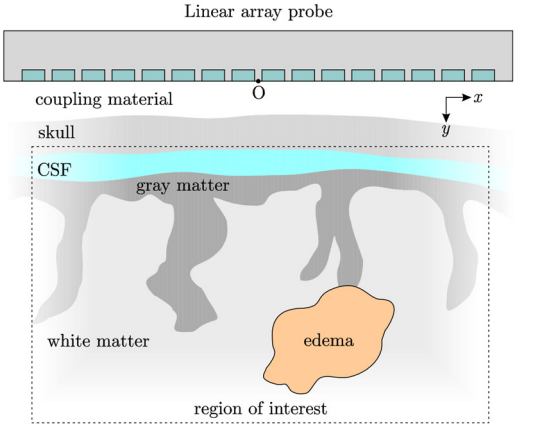

Figure 8.
Second simulation setup with a realistic brain region containing an edema

c_{skull} = 2,600 m/s, placed at a distance of h = 6mm from the transducer is included. Finally, the central simulation frequency is selected to be 1 MHz.

Initially, the simulation is performed in the absence of the skull, and an amount of noticeable artifacts, after the appropriate image reconstruction in Figure 7(a), is revealed as "wings" near the scatterer. Apparently, their intensity is considerably lower, yet they constitute a serious reason for an erroneous diagnosis. Then, the skull is included in our simulations, and the image is reconstructed via the conventional TFM scheme in Figure 7(b). As a first remark, we can point out the effective elimination of most artifacts; nonetheless, the edema region is significantly misaligned and distorted, as the increased acoustic velocity of the skull is not taken into account. To circumvent these hindrances, we apply our enhanced technique and reconstruct the image in Figure 7(c), attaining the fully corrected alignment and perfectly maintained shape of the edema region (scatterer) as well as the totally eliminated artifacts in the computational domain.

3.2 Realistic brain region

The second arrangement refers to the more realistic scenario of Figure 8, where the acoustic properties of all included tissues are summarised in Table 1. The average thickness of the

Material	Hydrogel	Bone	CSF	Grey matter	White matter
Acoustic velocity (m/s) c	1,540	2,600	1,500	1,550	1,600
Density (kg/m^3) ρ	1,000	1,900	1,000	1,050	1,030
Attenuation coefficient (dB/cm) α	0.002	11	0.8	0.8	0.8
Absorption power	1.5	0.6	1.5	1.1	1.1

Source: Van Venrooij *et al.* (1979), Bamber (1997), Clement *et al.* (2004)

Table 1. Acoustic properties of coupling material and human head tissues and skull at 1 MHz

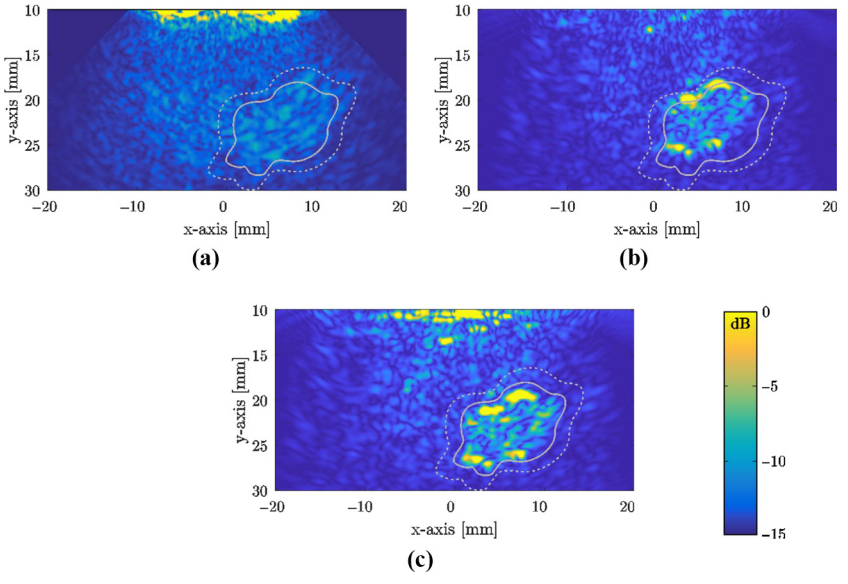

Figure 9. Image reconstruction of the setup depicted in Figure 8 via (a) a conventional phased array system, (b) the standard TFM technique and (c) the proposed scheme; the continuous line indicates the edema region and the dashed line shows the surrounding region for the CNR calculation

skull is approximately 5 mm, and the central simulation frequency is set to 2 MHz for improved resolution. Herein, the image reconstruction capabilities of the proposed scheme are compared to those of the standard TFM technique and a conventional phased array method. Note that the typical parameters – such as the number, size and location of the sensors as well as the time-gain compensation – of all systems remain the same to guarantee a fair comparison. In this context, the acquired images are illustrated Figure 9, and, as observed, all methods manage to unveil the edema existence. However, the contrast of the conventional phased array sensor is significantly degraded, as the skull thickness is 5 mm, unlike the usual-phased array application to a 2 mm thick temporal bone.

Moreover, similarly to the first setup, the standard TFM scheme fails to successfully align the edema scatterer since the skull acoustic velocity is not considered. Conversely, the featured methodology accomplishes the desired imaging outcomes, thus validating its reliable and very accurate transcranial application. Conversely, the featured methodology accomplishes the desired imaging outcomes. The prior observations can also be qualitatively substantiated by introducing an image quality quantification gauge, namely, the contrast-to-noise ratio (CNR) (Desai *et al.*, 2010):

$$\mathrm{CNR} = 10\log\frac{|S_A - S_B|}{\sigma_N}, \tag{11}$$

where S_A is the mean value of the intensity at the edema region (area limited by the continuous line in Figure 9), S_B is the mean value of the intensity at the surrounding region (area between the continuous and dashed line in Figure 9) and σ_N is the standard deviation of the background noise. The CNR for the examined cases is calculated 1.12 dB, 4.78 dB and 7.2 dB for the conventional phased array, the standard TFM and the proposed scheme, respectively. It becomes apparent that these values clearly indicate the superior performance of our technique incorporating the virtual source concept and reveal the significant improvement in the quality of the reconstructed image.

4. Conclusion

The enhanced and trustworthy transcranial ultrasonic imaging of the human brain via a rigorous TFM-based technique has been presented in this paper. The new method combines the focussing, because of the skull, of the initially spherical acoustic wave with the traditional TFM, by introducing an efficient virtual source, particularly tailored to the skull's increased acoustic velocity. Numerical results, addressing real-world biomedical setups, unveil that although the back-scattered signal is slightly weaker, the final image is reconstructed with a very promising accuracy and enhanced contrast, unlike the corresponding findings of existing approaches, such as the conventional phased array system that is restricted only to thin skull regions, e.g. the temporal bone.

References

Bae, M.H. and Jeong, M.K. (2000), "A study of synthetic-aperture imaging with virtual source elements in B-mode ultrasound imaging systems", *IEEE Transactions on Ultrasonics, Ferroelectrics, and Frequency Control*, Vol. 47 No. 6, pp. 1510-1519.

Bamber, J.C. (1997), *Acoustical Characteristics of Biological Media. Encyclopaedia of Acoustics*, Vol. 4, Wiley, New York, NY, pp. 1703-1726.

Behnke, S., Berg, D., Naumann, M. and Becker, G. (2005), "Differentiation of Parkinson's disease and atypical parkinsonian syndromes by transcranial ultrasound", *Journal of Neurology, Neurosurgery and Psychiatry*, Vol. 76 No. 3, pp. 423-425.

Berg, D. and Becker, G. (2002), "Perspectives of B-mode transcranial ultrasound", *NeuroImage*, Vol. 15 No. 3, pp. 463-473.

Clement, G.T. and Hynynen, K. (2002), "A non-invasive method for focusing ultrasound through the human skull", *Physics in Medicine and Biology*, Vol. 47 No. 8, p. 1219.

Clement, G.T., White, P.J. and Hynynen, K. (2004), "Enhanced ultrasound transmission through the human skull using shear mode conversion", *The Journal of the Acoustical Society of America*, Vol. 115 No. 3, pp. 1356-1364.

Desai, N., Singh, A. and Valentino, D.J. (2010), "Practical evaluation of image quality in computed radiographic (CR) imaging systems", in *Proceeding Medical Imaging 2010: Physics of Medical Imaging, International Society for Optics and Photonics*, Vol. 7622, p. 76224Q.

Eichardt, R., Strohmeier, D., Hunold, A., Machts, R., Haueisen, J., Oelsner, G., Schmidt, C., Schultze, V., Stolz, R. and Graichen, U. (2019), "Sensitivity studies and optimization of arrangements of optically pumped magnetometers in simulated magnetoencephalography", *COMPEL – The International Journal for Computation and Mathematics in Electrical and Electronic Engineering*, Vol. 38 No. 3, pp. 953-964.

Godau, J. and Berg, D. (2010), "Role of transcranial ultrasound in the diagnosis of movement disorders", *Neuroimaging Clinics of North America*, Vol. 20 No. 1, pp. 87-101.

Holmes, C., Drinkwater, B. and Wilcox, P. (2004), "The post-processing of ultrasonic array data using the total focusing method", *Insight – Non-Destructive Testing and Condition Monitoring*, Vol. 46 No. 11, pp. 677-680.

HöLscher, T., Wilkening, W.G., Molkenstruck, S., Voit, H., and and Koch, C. (2008), "Transcranial sound field characterization", *Ultrasound in Medicine and Biology*, Vol. 34 No. 6, pp. 973-980.

HöLscher, T., Wilkening, W., Draganski, B., Meves, S.H., Eyding, J., Voit, H., Bogdahn, U., Przuntek, H., and and Postert, T. (2005), "Transcranial ultrasound brain perfusion assessment with a contrast agent-specific imaging mode: results of a two-center trial", *Stroke*, Vol. 36 No. 10, pp. 2283-2285.

International Organization for Standardization ISO (2019), Non-Destructive Testing. Ultrasonic Thickness Measurement, BS EN ISO Standard No. 16809:2019.

Jensen, J.A., Nikolov, S.I., Gammelmark, K.L. and Pedersen, M.H. (2006), "Synthetic aperture ultrasound imaging", *Ultrasonics*, Vol. 44, pp. e5-e15.

Kraiger, M. and Schnizer, B. (2013), "Potential and field of a homogeneous magnetic spheroid of arbitrary direction in a homogeneous magnetic field in Cartesian coordinates", *COMPEL – The International Journal for Computation and Mathematics in Electrical and Electronic Engineering*, Vol. 32 No. 3, pp. 936-960.

Le Jeune, L., Robert, S., Dumas, P., Membre, A. and Prada, C. (2015), "Adaptive ultrasonic imaging with the total focusing method for inspection of complex components immersed in water", *Proceeding 2015 AIP Conference*, Vol. 1650 No. 1, pp. 1037-1046.

Lindsey, B.D., Light, E.D., Nicoletto, H.A., Bennett, E.R., Laskowitz, D.T. and Smith, S.W. (2011), "The ultrasound brain helmet: new transducers and volume registration for in vivo simultaneous multi-transducer 3-D transcranial imaging", *IEEE Transactions on Ultrasonics, Ferroelectrics and Frequency Control*, Vol. 58 No. 6, pp. 1189-1202.

Lockwood, G.R., Talman, J.R. and Brunke, S.S. (1998), "Real-time 3-D ultrasound imaging using sparse synthetic aperture beamforming", *IEEE Transactions on Ultrasonics, Ferroelectrics and Frequency Control*, Vol. 45 No. 4, pp. 980-988.

Mast, T.D., Souriau, L.P., Liu, D.L., Tabei, M., Nachman, A.I. and Waag, R.C. (2001), "A k-space method for large-scale models of wave propagation in tissue", *IEEE Transactions on Ultrasonics, Ferroelectrics and Frequency Control*, Vol. 48 No. 2, pp. 341-354.

Oldendorf, W.H. (1978), "The quest for an image of brain: a brief historical and technical review of brain imaging techniques", *Neurology*, Vol. 28 No. 6, pp. 517-517.

Shenton, M.E., Hamoda, H.M., Schneiderman, J.S., Bouix, S., Pasternak, O., Rathi, Y., Vu, M.A., Purohit, M.P., Helmer, K., Koerte, I., Lin, A.P., Westin, C.F., Kikinis, R., Kubicki, M., Stern, R.A. and Zafonte, R. (2012), "A review of magnetic resonance imaging and diffusion tensor imaging findings in mild traumatic brain injury", *Brain Imaging and Behavior*, Vol. 6 No. 2, pp. 137-192.

Szajerman, D., Napieralski, P. and Lecointe, J. (2018), "Joint analysis of simultaneous EEG and eye tracking data for video images", *COMPEL – The International Journal for Computation and Mathematics in Electrical and Electronic Engineering*, Vol. 37 No. 5, pp. 1870-1884.

Tabei, M., Mast, T.D. and Waag, R.C. (2002), "A k-space method for coupled first-order acoustic propagation equations", *The Journal of the Acoustical Society of America*, Vol. 111 No. 1, pp. 53-63.

Treeby, B.E. and Cox, B.T. (2010), "k-Wave: MATLAB toolbox for the simulation and reconstruction of photoacoustic wave fields", *Journal of Biomedical Optics*, Vol. 15 No. 2, p. 021314.

Van Venrooij, G.E.P.M., Boone, R.M. and Dernier van der Gon, J.J. (1979), "Two-dimensional echo-encephalography", *Acta Neurochirurgica*, Vol. 49 Nos 1/2, pp. 1-8.

Vignon, F., Aubry, J.F., Tanter, M., Margoum, A. and Fink, M. (2006), "Adaptive focusing for transcranial ultrasound imaging using dual arrays", *The Journal of the Acoustical Society of America*, Vol. 120 No. 5, pp. 2737-2745.

Vignon, F., Aubry, J.F., Tanter, M., Margoum, A., Fink, M. and Lecoeur, J.M. (2005), "Dual-arrays brain imaging prototype: experimental in vitro results", in *Proceeding 2005 IEEE Ultrasonics Symposium*, Vol. 1, pp. 504-507.

Wintermark, M., Sesay, M., Barbier, E., Borbély, K., Dillon, W.P., Eastwood, J.D., Glenn, T.C., Grandin, C.B., Pedraza, S., Soustiel, J.F., Nariai, T., Zaharchuk, G., Caillé, J.M., Dousset, V. and Yonas, H. (2005), "Comparative overview of brain perfusion imaging techniques", *Stroke*, Vol. 36 No. 9, pp. e83-e99.

Zhang, J., Drinkwater, B.W., Wilcox, P.D. and Hunter, A.J. (2010), "Defect detection using ultrasonic arrays: the multi-mode total focusing method", *NDT and E International*, Vol. 43 No. 2, pp. 123-133.

Zhang, Y., Ren, Z. and Lautru, D. (2014), "Finite element modeling of current dipoles using direct and subtraction methods for EEG forward problem", *COMPEL – The International Journal for Computation and Mathematics in Electrical and Electronic Engineering*, Vol. 33 Nos 1/2, pp. 210-223.

Corresponding author
Stamatis A. Amanatiadis can be contacted at:samanati@auth.gr